WARSAW UNIVERSITY OF TECHNOLOGY Index 351733
FACULTY OF CIVIL ENGINEERING
COMMITTEE FOR CIVIL AND WATER ENGINEERING
POLISH ACADEMY OF SCIENCES ISSN 1230-2945

DOI: 10.24425/ace.2025.153345
ARCHIVES OF CIVIL ENGINEERING
Vol. LXXI ISSUE 1 2025
pp. 469–487

Research paper

Pre-camber control of large-span prestressed concrete continuous rigid-frame bridges under cantilever construction

Yingying Zhou[1]

Abstract: In the commonly used cantilever construction method, the construction is greatly affected by the linearity and stress control, and the failure of linearity and stress control will lead to the deformation of the bridge. To solve this problem, the study carried out finite element analysis modeling of large-span prestressed concrete continuous rigid bridge, and measured the creep coefficient by creep test to determine the model parameters. The experimental results show that. When the self weight of concrete is 1.10γ. At that time, the deflection variation at the cantilever end of the main beam reached its maximum value near the mid span and side span merging sections, which were 8.6 mm and 9.7 mm, respectively. In the max cantilever state, increasing the concrete capacity decreases the compressive stress at the upper and lower edge of the cross-section to 1.18 MPa and 1.24 MPa, respectively. In the bridge-forming state, increasing the concrete deadweight results in a decrease in the normal stress at the upper and lower edges of the bridge to 1.24 and 1.27, respectively, while the normal stress at the lower edge of the cross-section remains unchanged. The creep modification model obtained from the creep test is able to predict the deformations and stresses of the cantilevered construction of a continuous rigid bridge with a more accurate prediction.

Keywords: cantilever construction, linear control, long span bridge, rigid frame bridge, stress control

[1]Mas., Henan Institute of Construction Technology, Zhengzhou, 450064 China, e-mail: zyy76691176@163.com, ORCID: 0009-0005-8330-4345

1. Introduction

With the rapid development of global urbanization and transportation networks, large-span bridges are becoming an important part of transportation infrastructure. According to the International Bridge and Tunnel Association (IBTA), the amount of new large-span prestressed concrete continuous rigid-frame bridges (PCCRF bridges) has increased by about 40% in the past five years. In China, this figure is as high as 60%. These bridges not only serve as important nodes for transportation, but also become landmarks for cities and regions. However, large-span PCCRF bridges face many challenges during construction, especially during the cantilever construction phase. According to recent engineering case studies, inaccurate alignment control may lead to uneven deformation of the bridge, which in turn affects the load carrying capacity and service life of the bridge [1]. For example, in the past three years, at least five large-span PCCRF bridges around the world experienced structural problems due to inappropriate alignment control, leading to emergency repairs or even bridge closure. Cantilever construction is a commonly used method of construction for large-span bridges, but its inherent instability makes alignment and stress control an important aspect of construction safety. Inaccurate alignment control may lead to uneven deformation of the bridge, which in turn affects the bearing capacity and service life of the bridge [2]. Meanwhile, inappropriate stress control may also lead to loss of prestressing or member damage, thus increasing project risks and maintenance costs. According to statistics, such problems cause billions of dollars of economic losses to the global infrastructure every year [3]. Therefore, the aim of this study is to deeply investigate the alignment and stress control problems of large-span PCCRF bridges in cantilever construction. By analyzing and comparing the actual engineering cases, as well as using advanced monitoring and simulation techniques, numerical simulation analysis of line shape and stress is conducted to provide powerful technical support for similar projects in the future.

The study is divided into four parts, the first part of which introduces the necessity of linear and stress control for large-span PCCRF bridges, the second part of which proposes the scheme and parameters for linear and stress prediction by finite element analysis (FEA), and conducts concrete creep test to measure the creep coefficients, and the third part of which conducts the test and analysis of actual engineering cases; the fourth part of which summarizes the above content.

2. Related works

Highway and bridge construction is a support facility for basic economic construction, and a large amount of scholars have carried out relevant research on it. Reymert et al. studied systematic literature search, mapping and data analysis to reduce the hazards of extreme weather on large-span bridges in the community and to avoid the resulting traffic safety problems, and proposed a new traffic safety calculation model and simulation procedure, which was proved by experiments to be able to efficiently predict the vehicles in the operating environment on bridges and estimate wind conditions and vehicle aerodynamic loads [4]. Siwowski et al. proposed

a FRP composite lightweight concrete structure and validated the proposed structure through finite element analysis. Researchers conducted comparative experiments on the stiffness, strength, and dynamic performance of the proposed structure using finite element analysis. The experimental results showed that linear finite element can achieve the bending resistance of hybrid bridge systems. This result proves that the structure proposed in the study meets the requirements and standards related to bridges, therefore the study has practical significance [5]. Ma et al. studied the green fiber-reinforced concrete used in highway bridges and its physical and mechanical properties over time, proposed a calculation method for the physical and mechanical properties of green fiber-reinforced concrete, and tested its physical and mechanical properties, and the experimental results proved that the green fiber-reinforced concrete has good physical properties and durability [6]. Dai et al. proposed an extreme value analysis method for predicting extreme load effects and multiple presence coefficients of highway-railway bridges in order to calculate multiple presence coefficients of integrated road traffic loads in modern cities, which is an unsupervised clustering algorithm based on the generalized extreme value mixture model, and predicts the extreme values by fitting the mixed distribution feature data, and the experimental results show that this method is more reliable than the traditional generalized extreme value method [7]. Cosenza et al. proposed a safety assessment and performance rating evaluation model suitable for reinforced concrete bridges based on the newly proposed Italian Guidelines for Risk Classification, Safety Assessment and Structural Health Monitoring of Existing Bridges to evaluate the risk elimination and safety assessment of existing reinforced concrete bridges, which proved the complete validity of the evaluation model [8].

The research on linear and stress control is generally focused on the field of concrete materials, engineering and construction, and metal materials, etc. Zhu et al. used torsional predeformation (TPD) treatment to achieve biphasic control of austenite and martensite in order to improve the temperature stability of shape memory alloys (SMAs) over a wide temperature range. The results showed that after TPD treatment, the residual martensite phase in the samples showed a gradient distribution with unit torsion angles ranging from 0.75 to 3.75 degrees/mm. The biphasic structure after TPD can suppress the temperature dependence of the superelastic stresses in the SMAs while maintaining the pronounced superelasticity [9]. Monjusha et al. explored the use of iron-based SMA ribbons for the repair after seismic strengthening of RC abutment models. The experimental results showed that the abutment specimens with Fe-SMA reinforcement in the form of EA showed enhanced load carrying capacity but less improvement in ultimate displacement, whereas the Fe-SMA rings improved the ultimate displacement of the specimens with less improvement in peak lateral load. the combination of EA and ring Fe-SMA reinforcement was found to be more effective in improving all seismic performance parameters [10]. Kang et al. aimed to investigate the effect of pit characterization parameters on the mechanical properties and fracture modeling of wire ropes. Tensile tests and FEA were carried out on wires with corrosion damage to investigate the development of wire stresses in the corroded form. The experiment findings indicated that with the increase of corrosion, the necking phenomenon of the wire is not obvious, and the crack originates near the pit bottom and extends to the inside of the specimen. The fiber region of the corroded wire decreases while the radiation region increases, and the ductile fracture gradually changes to brittle fracture [11].

Although a large amount of studies have focused on the design and construction of prestressed concrete bridges, relatively few studies have been conducted on the alignment and stress control of large-span PCCRF bridges in cantilever construction. In addition, most of the existing studies are based on theoretical analysis and numerical simulation, and lack the verification of practical engineering applications.

3. Linear and stress prediction modeling of large-span prestressed concrete continuous rigid-frame bridges

In the field of bridge construction, there is a need to ensure that the alignment and stress control meet the requirements of structural safety and design alignment. The cantilever construction process for continuous rigid frame bridges is particularly complex, with the linear shape and internal forces of the bridge structure constantly changing as the number of cantilever segments increases. However, due to the influence of factors such as weight of embedded concrete, modulus of elasticity, temperature change and shrinkage creep, as well as operational errors during the construction process, the actual structural state may deviate from the theoretical design state. If these errors are not adjusted, larger deviations will be accumulated in the next stage, leading to serious deviations in the bridge alignment and inconsistencies in the internal forces, which may ultimately lead to difficulties in joining the bridge.

3.1. Construction of finite element analysis model for large-span prestressed concrete continuous rigid-frame bridge construction

The prestressed concrete continuous rigid frame bridge (referred to as the continuous rigid frame bridge) is a type of prestressed concrete box structure bridge derived from the continuous beam and T-shaped rigid frame foundation with the development of prestressed technology and cantilever construction technology [12]. Among them, prestressing is achieved by pre applying pressure to the structure before it bears the load. This pre applied pressure can partially or completely offset the tensile stress caused by external loads, thereby avoiding or at least delaying the occurrence of cracks in the structure during normal use. under advisement. The span structure of a continuous rigid frame bridge is a prestressed concrete continuous box beam, with the main pier mostly using hollow thin-walled or double thin-walled piers, and the box beam body is consolidated with the thin-walled bridge pier. Continuous rigid frame bridges integrate the main advantages of continuous beam bridges and T-shaped rigid frame bridges, and effectively avoid their drawbacks [13]. Continuous rigid frame bridges not only have the advantages of small deformation, good structural stiffness, smooth driving, fewer expansion joints, simple maintenance, and good seismic performance of the continuous beam bridge structural system, but also have the characteristics of T-shaped rigid frame bridges with no support for the main pier, easy cantilever pouring, favorable for mechanized construction, and the ability to develop towards larger spans.

The main task of bridge construction control is to accurately control the structural alignment (construction pre-camber, finished bridge pre-camber, construction deflection, line shape for design) and internal force during the construction process, through theoretical calculation and analysis of each construction section, optimize the parameters according to the results of the analysis, reduce the error, and provide more reasonable data for the next stage, in order to achieve the ideal alignment and structural internal force state. Construction control of structural alignment control is the core content, and its goal is to realize the linear state of bridge formation stipulated in the construction drawings, focusing on the main girder axis control and vertical displacement control of the bridge structure [14, 15]. Specific operations include real-time theoretical calculation and analysis, adjusting the elevation of the main girder cantilever forward end mold and control parameters according to the analysis results and measured data, as well as subsequent error analysis and adjustment. The structural stress control is designed to ensure the safety of the bridge structure, and the stress monitoring process is shown in Fig. 1.

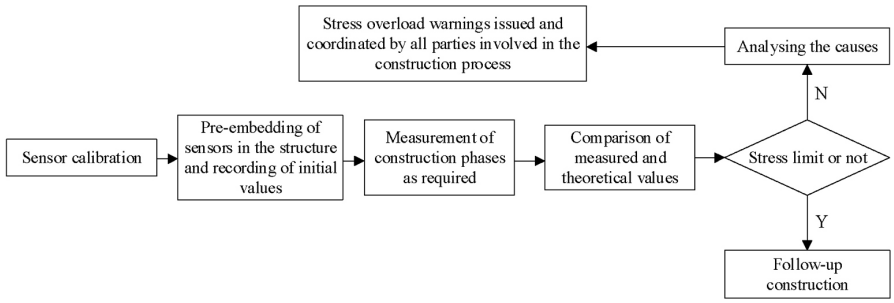

Fig. 1. Stress monitoring process

The stress monitoring process is shown in Fig. 1. Firstly, according to the FEA, the key section is selected and the stress is monitored in real time by burying strain gauges. After the data collection, it is compared with the theoretical value, and if there is any deviation, the error source is analyzed and the parameters are adjusted in the next stage to reduce the error. This process needs to be carried out cyclically to ensure that the stress control at each construction stage meets the design requirements. At the same time, strict records of stress control are kept for later evaluation and adjustment. Structural stability control focuses on stability calculation and analysis at critical construction stages to address the complex force conditions of a continuous rigid-frame bridge, and ensures the stability of temporary and ancillary structures. These three aspects of control are systematically monitored and adjusted to ensure that the internal forces and deformations of the bridge in the cantilevered state and the finalized state meet the allowable error range. The construction of the continuous rigid-frame bridge needs to be completed stage by stage to ensure that the alignment and stresses of each stage are in accordance with the design, and that the next construction stage is guided by appropriate calculation and analysis methods through accurate prediction and monitoring until the structure is merged. The stress calculation formula is shown in Eq. (3.1).

$$\sigma = \frac{M}{S} + P/A \tag{3.1}$$

In Eq. (3.1), σ denotes the stress, M denotes the bending moment, S is the section modulus, P denotes the prestress, and A is the section area. The relationship between stress and strain is shown in Eq. (3.2).

$$\varepsilon = \frac{\sigma}{E} \tag{3.2}$$

In Eq. (3.2), E denotes the modulus of elasticity, E denotes the strain. In the cantilever construction of continuous rigid-frame bridges, the self-weight of concrete, prestressing tension, modulus of elasticity and concrete shrinkage and creep affect the internal force and deformation of the structure, resulting in the bridge deviating from the design elevation. In order to achieve the precision of merging and to ensure that the bridge line conforms to the design, it is necessary to adjust the elevation of each section of the vertical mold in real time according to the actual construction situation. The calculation formula for determining the elevation of bridge standing mold is shown in Eq. (3.3).

$$H_{lm}^{i} = H_{\text{design}}^{i} + H_{cq}^{i} + H_{sg}^{i} + H_{gl}^{i} + H_{\text{construction}}^{i} \tag{3.3}$$

In Eq. (3.3), H_{lm}^{i} represents the elevation of the section i, H_{design}^{i} represents its design height, H_{cq}^{i} represents the pre-arch degree of the wall, H_{sg}^{i} represents the construction deformation, H_{gl}^{i} represents the deformation of the hanging basket, and $H_{\text{construction}}^{i}$ represents the amount of elevation adjustment in order to adjust the cumulative lineal error of the construction. In the linear control of construction, focusing on the control of structural axis and deflection, the observation point is laid in the front end of the bridge cantilever, the location is shown in Fig. 2.

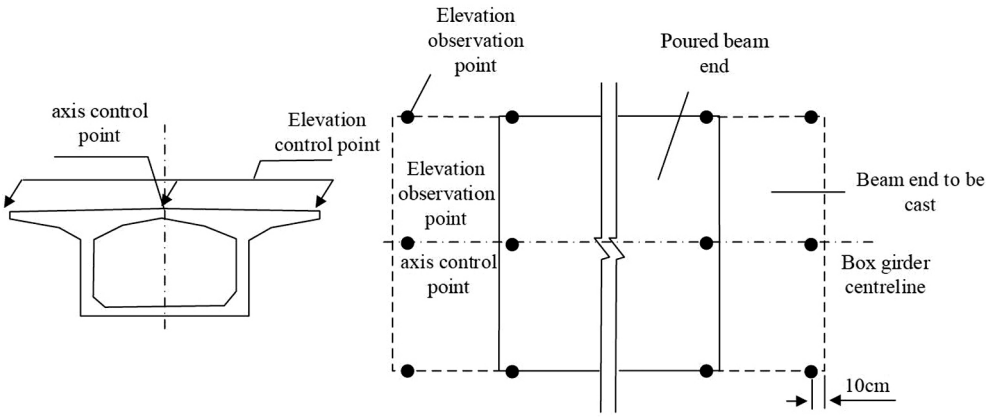

Fig. 2. Location of observation points: (a) Cross-sectional maps, (b) Floor plan

In the stage of structure construction to the top of the pier, the main girder alignment control and measurement work is initiated. First of all, the main girder measurement control points were established at the center of the pier top through the measurement control points

on both sides of the bridge, as the level base point for elevation. Deflection measurements were carried out in three stages before and after concrete pouring and after prestressing beam tensioning, covering the measurement points on the side span side and the center span side of the cantilever block section. Since temperature change has a significant effect on the structural deflection, the elevation measurement should be carried out in the early morning when the temperature change is the smallest, and after each measurement, the data should be remeasured in the evening to compare and analyze the data, so as to reduce the error and improve the accuracy. With the increase of cantilever casting blocks, the deformation of the structure increases gradually, each measurement should cover the newly cast and adjacent cantilever blocks, and the constructed segments should be comprehensively inspected regularly to ensure that the structural axis and deflection comply with the design requirements [16]. The stress monitoring points of the finite element simulation model are set in the structural cantilever root section, one-half of the cantilever length section, and the merging section, in order to measure the concrete strain and compare with the model, and the arrangement of the stress measurement points is shown in Fig. 3.

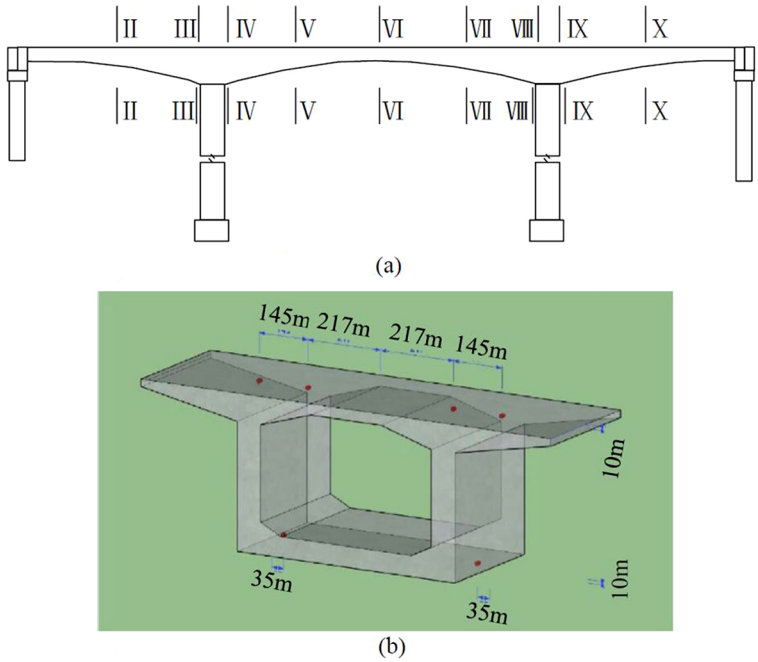

Fig. 3. Stress measurement point arrangement: (a) Cross-section layout of stress measurement points, (b) Layout of cross-section measurement points

Stress and strain monitoring measurements were critical during all phases of structural construction. Prior to the placement of concrete in Block Zero, smart chord digital transducers were tied to the longitudinal reinforcement in the top and bottom slabs of the control section at the root of the box girder. During the cantilever construction of the main girder, strain

measurements needed to be monitored several times over time, especially at critical stages before and after the concrete placement and after the prestressing strand tensioning was completed. If the measurement results are consistent with the model calculations, the strain readings can be appropriately reduced during subsequent stress monitoring. The density of stress monitoring should be strengthened during the critical construction stages of side span and center span merging. To minimize the influence of temperature changes on the test results, stress measurements should be arranged in the early morning when the temperature changes are small, and real-time ambient temperature should be measured at the same time to ensure the accuracy of the test results. The study was conducted to control the alignment and stress of the spanwise prestressed concrete continuous rigid bridge, to construct a simulation model of its cantilever construction process, and to establish a finite element model of the whole bridge for numerical analysis. The study selected the Jinyang River Extra Large Rigid Frame Bridge in the western Sichuan Basin as a reference for simulation model construction. The simulation model construction adopts the finite difference method to construct the finite element model of the bridge through geometric modeling in Autodesk CFD. The modeling elements are selected as solid elements, and the bridge foundation is made of rock, and the bridge deck is made of steel bars and concrete. The model has a plane size of 757.7m x 50m and a thickness of 10m. The prestressed reinforcement is mainly distributed in the pile foundation of the bridge deck and piers, and the specific distribution of prestressed reinforcement is shown in the blue part of Fig. 4. The influence of prestressing on concrete components is calculated using a sub item method and superimposed. In the model, there are a total of 92 beam elements, and the detailed 3D model is shown in Fig. 4.

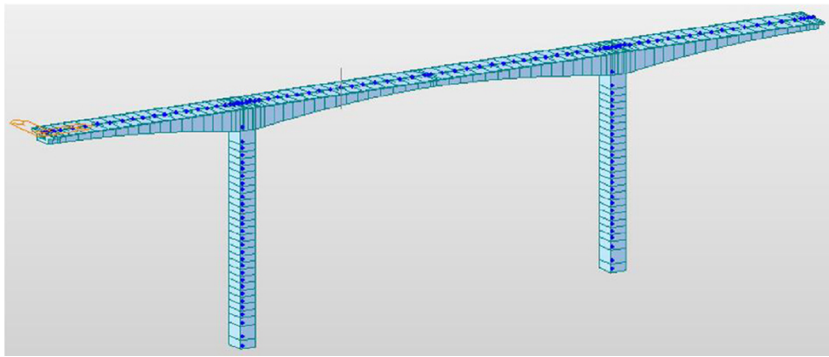

Fig. 4. Three-dimensional model for finite element analysis

The cantilever construction of span PCCRF bridges is complicated, with the increase of segments, the structural deformation and internal force change constantly, and many factors lead to the difference between the actual structural state and the theoretical design. FEA is an important means of bridge construction control, which can accurately calculate and analyze for each construction stage, providing scientific basis for optimizing parameters, reducing errors, and ensuring construction safety and structural stability. Due to the symmetry of the left and right sides of the bridge during the model construction process, in order to facilitate

the description of the results, the study selected the right main bridge, right bridge pier, and two parts, simulated the construction phase according to the actual construction sequence, and inspected the structure of the bridge. Among them, the box girder adopts box section prestressed structural beam unit, and the abutment adopts box section reinforced concrete structural beam unit. The simulation model of FEA is able to analyze the dynamic changes of deflection and stress during the cantilever construction of the PCCRF bridges. With the increase of the cantilever concrete block section, the vertical deflection of the main pier cantilever gradually increases, and the maximum value appears at the maximum cantilever end of the side span. After tensioning prestressing, the vertical deflection decreases, and the main change of deflection originates from concrete casting and prestressing tensioning, and the deformation of these two working conditions needs to be strictly controlled. At the same time, the study also needs to analyze the cross-sectional stress at the root of the cantilever at different construction stages. If the stress at the upper and lower edges of the cross-section at each construction stage is within a reasonable range, it indicates that the construction meets expectations. Study the pouring and pre embedding of prestressed reinforcement for each block segment, and observe the stress changes in each part. After pre embedding prestressed reinforcement, the pre stress value of the model gradually increases, the upper stress increases, and the lower compressive stress decreases. The basic parameters of the structure for FEA were calculated according to the project information, and the physical properties of the prestressed concrete and the mechanical properties of the prestressing tendons are shown in Table 1.

Table 1. Physical properties of prestressed concrete materials and mechanical properties of tendons

Concrete Material Properties	**Numeric size**	**Mechanical properties of prestressing tendons**	**Numeric size**
Modulus of elasticity of concrete	35500 MPa	Modulus of elasticity	195000 MPa
Concrete weight	26 kN/m	Orifice deviation factor	0.0015
Coefficient of linear expansion of concrete	0.00001	Beam relaxation factor	0.3
Poisson's ratio	0.2	Coefficient of friction of prestressing orifices	0.17
Strength of prestressed concrete	≥ 95%	telescoping	0.006 m
–	–	Longitudinal beam tensioning control stress	l395 MPa
–	–	Transverse beam tensioning control stress	1302 MPa
–	–	Vertical beam tensioning control stress	785 MPa

3.2. Design of concrete creep test for large-span prestressed rigid bridges

Structural deflection and stress have the greatest influence on the creep effect of concrete. Considering that the different aggregate in different places have a great influence on the working efficiency, mechanical properties, durability and shrinkage creep of concrete, in order to improve the accuracy of the simulation model, the creep test was carried out on the local mechanized sand concrete in order to update the prediction model for the concrete creep, and the experimental process is shown in Fig. 5.

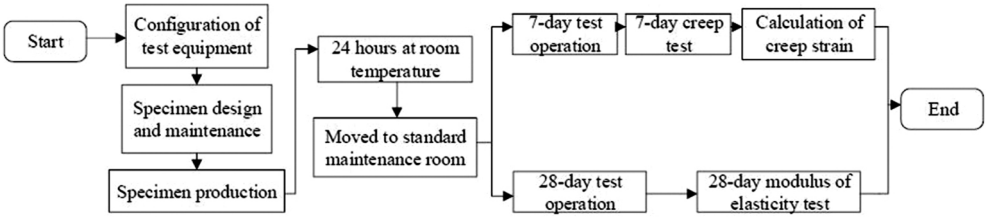

Fig. 5. Flow of creep test

According to the provisions of the Standard for Long-term Performance and Durability Test Methods for Ordinary Concrete (GB/T50082-2009), a series of test equipment was firstly configured, including microcomputer-controlled electro-hydraulic servo press LX002, forced single-horizontal-axis concrete mixer HNT003, slump meter HNT004, hydraulic jacks, spring-type compression creep apparatus, and load sensors, strain gauges and sensors, etc. In terms of specimen design and maintenance, different sizes of specimens were made according to the regulations, including cubic compression specimen, axial compression specimen, modulus of elasticity specimen, shrinkage strain specimen, and creep strain specimen, and at least two specimens were selected as a group to be tested for each type of test [17]. The testing process requires 7 and 28 days of curing at specific temperatures and humidity. After the maintenance is completed, the axial compressive strength and elastic modulus of the specimens cured for 7 days and 28 days shall be measured and evaluated respectively, until the creep test is completed. The concrete steps of the creep test include the compressive strength test and elastic modulus test of the prism at the age of 7 days. During the test, the instrument needs to be checked and relevant sensors installed. At the same time, it needs to be stacked together for centering adjustment to facilitate the final reading of data. Subsequently, gradually loaded to 20% of the 7-day axial compressive strength for loading and centering adjustments to ensure that the difference in force between the two sides of the specimen is within 10% of the average value, adjusted to the creep stress, and recorded the average of the deformation on both sides as the initial deformation value [18, 19]. When the creep test is carried out, measure the deformation readings of two groups of shrinkage specimens under the same maintenance conditions, check the maintenance of the creep test load periodically, and make up for the change in creep stress if it is greater than 2%. The formula for calculation of creep strain is shown in Eq. (3.4).

$$\varepsilon_{ct} = \frac{L_t - L_0}{L_b} - \varepsilon_t \tag{3.4}$$

In Eq. (3.4), ε_{ct} and L_t denote the creep strain after loading t, L_0 denotes the initial deformation value before loading, L_b denotes the measurement distance, and ε_t denotes the shrinkage value at the same age. The initial strain value before loading is calculated in Eq. (3.5).

$$\varepsilon_0 = \frac{\Delta L_0}{L_b} \tag{3.5}$$

The calculation of the creep coefficient φ_t based on Eq. (3.5) with loading t is shown in Eq. (3.6).

$$\varphi_t = \frac{\varepsilon_{ct}}{\varepsilon_0} \tag{3.6}$$

The data were processed in accordance with the arithmetic mean of the experimental results of the specimens for the determination of the creep coefficient of concrete specimens, and the creep prediction model was corrected after the determination of the test data. The creep prediction model adopts the CEB-FIP (1990) model for normal and high-strength concrete, in which the creep coefficient calculation formula is shown in Eq. (3.7).

$$\phi(t, t_0) = \phi_0 \left[\frac{t - t_0}{\beta_{RH} + t - t_0} \right]^a \tag{3.7}$$

In Eq. (3.7), t_0 represents the start time of the creep coefficient calculation; ϕ_0 denote the creep coefficients, which are affected by the theoretical thickness of the member, ambient humidity, concrete material, etc., β_{RH} denotes the coefficients related to the average relative humidity and the theoretical thickness of the member, and a denotes the coefficients related to time, and Eq. (3.8) is used to assign values to Eq. (3.7).

$$x = t - t_0 \tag{3.8}$$

Simplified by Eq. (3.8), there is a calculation shown in Eq. (3.9).

$$y = a \left[\frac{x}{b + x} \right]^c \tag{3.9}$$

Using Eq. (3.9) to compare with the actual measured data, a Xu-variation function applicable to the model was fitted.

4. Finite element analysis modeling of large-span prestressed concrete continuous rigid-frame bridge construction

A bridge under construction in Sichuan Province is selected as an engineering case, and its arrangement is shown in Fig. 6.

As shown in Fig. 6, the bridge is a left-right line separated arrangement bridge, the main bridge span arrangement is 134.4 + 500 + 123.3 m, with a total length of 757.7 m. The structural system of bridges mainly consists of upper structure, lower structure, expansion joints and

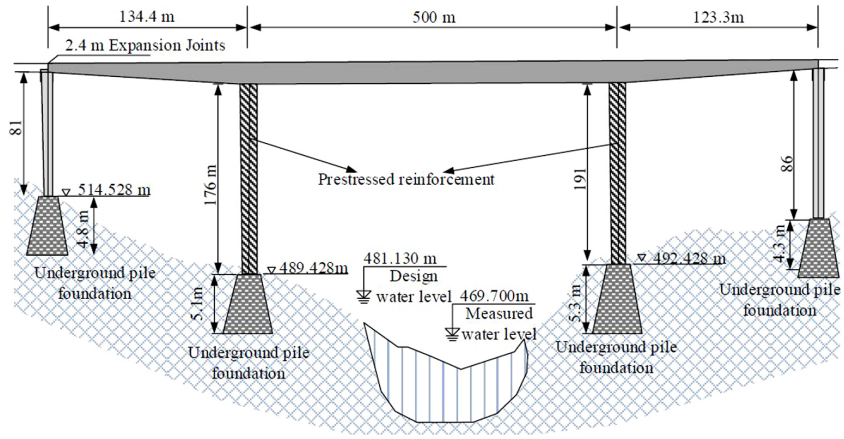

Fig. 6. Project case

supports, bridge deck pavement, and underground pile foundation. The upper structure is mainly designed as a single box and single box girder cross-section, with the main beam prestressed distributed in multiple directions. The width of the bridge deck is 12.25 m, the cross-sectional height of the top of the main pier is 7.2 m, and the cross-sectional height of the middle and side spans is 2.7 m. The height of the main girder varies according to 1.8 times parabola, the width of the top girder is 12.25 m, and the width of the bottom girder is 6.5 m. The construction of the box girder adopts traveler cantilever casting method, which is divided into 15 cantilever casting sections, and the longitudinal length of each section is 3×3 m $+7 \times 3.5$ m $+5 \times 4$ m in turn. Longitudinal prestressing adopts three types of steel bundles, whose standard tensile strength is 1860 MPa, and is divided into flat bending and vertical bending in two layout forms. Vertical prestressing steel bundle adopts JL32 fine-rolled threaded coarse steel bar with a standard strength of 785 MPa. The substructure mainly includes 3# and 4# main piers and 2# and 5# transition piers, all of which adopt rectangular hollow thin-walled section, in which the longitudinal and transversal cross-section size of the main piers is 5×6.5 m with a wall thickness of 70 cm, while the cross-section size of the transition piers is 6.5 m (transverse) $\times 3.0$ m (longitudinal) with a wall thickness of 60 cm. In the cantilever construction of continuous rigid bridge, in order to carry out the linear control and internal force control of the structure, it is necessary to accurately grasp the degree of influence of structural parameters on the structure, so the main parameters of the bridge structure are analyzed. Since the weight of the structure itself has the greatest influence on the deflection and stress, firstly, the deflection under different load capacity is analyzed based on the finite element model, and the outcomes are denoted in Fig. 7.

In order to compare the cantilever state and deflection difference of bridge structures under different bulk densities, the theoretical design value of assuming γ represents bulk density was studied, and the change of γ was set to three groups: –5%,+5%, and+10% for experimental purposes. The results are shown in Fig. 7. Figs. 7(a),(b) show the deflection differences between the maximum cantilever state and the completed bridge state under different bulk densities, respectively. The overall comparison shows that the deflection in the maximum cantilever state and the bridge-forming state increases gradually with the increase of the deadweight of

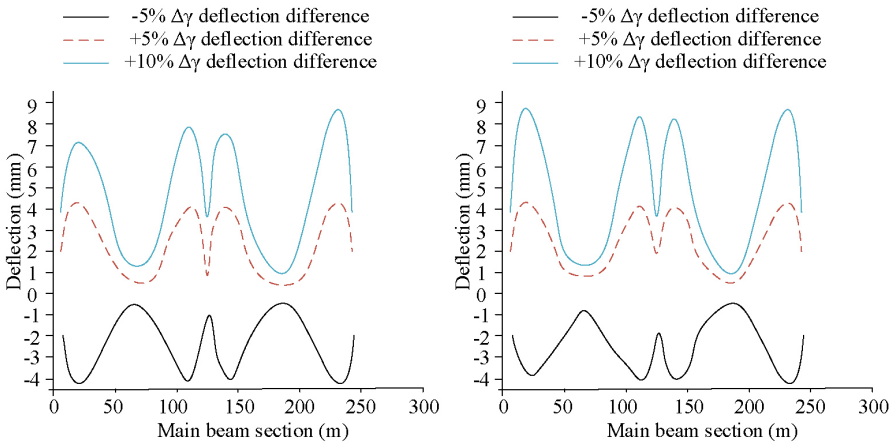

Fig. 7. Deflection analysis at different capacity weights: (a) Difference in deflection between the upper and lower edges of the cantilever state at different capacities, (b) Difference in deflection at bridge formation for different capacities

the structure. The deflection of the maximum cantilever state and the completed bridge state show the same trend as γ increases, while the trend is opposite as γ decreases. At the concrete capacity of 1.10 γ, the deflection change value of the cantilever end of the main girder reaches the maximum near the mid-span and side-span merging section, which is 8.6 mm and 9.7 mm, respectively, showing that the sensitivity to the deflection change in the finished condition is higher than that in the cantilever condition. The results of stress analysis under different capacities are shown in Fig. 8.

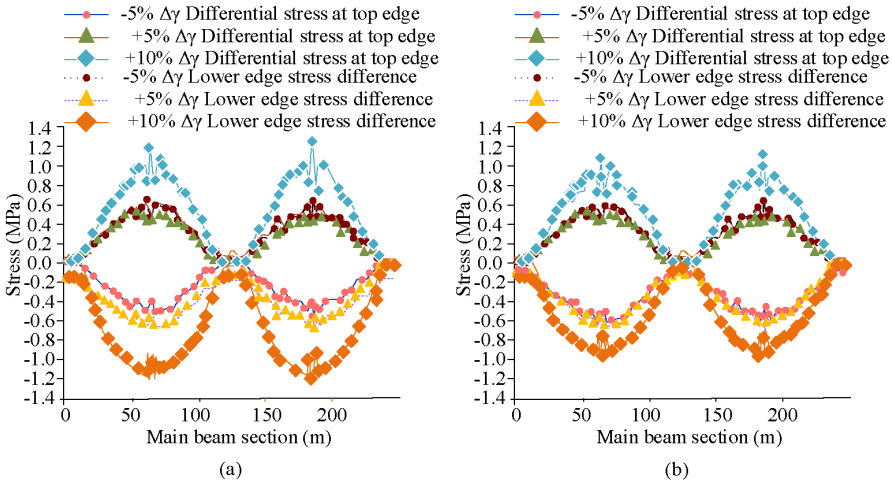

Fig. 8. Stress analysis at different bulk weights: (a) Difference in pressure between the upper and lower edges of the cantilever state at different load capacities, (b) Difference in stresses at the top and bottom edges in the bridge-formed condition at different capacities

Figure 8(a) shows the stress difference between the upper and lower edges of the bridge under different bulk densities. Fig. 8(b) shows the difference in stress between the upper and lower edges of the maximum cantilever state under different bulk densities. According to the results of Figs. 8(a),(b), it can be seen that if the bulk density of concrete is increased, the compressive stress at the upper edge of the section will decrease to 1.18 MPa, while the compressive stress at the lower edge of the section will increase to 1.24 MPa. In the completed bridge state, an increase in concrete bulk density will cause the normal stress at the upper edge of the main beam to decrease to 1.27 MPa, while the compressive stress at the lower edge remains unchanged. In addition to the structural weight, the modulus of elasticity of the concrete also has a great influence on the stiffened bridge. concrete modulus of elasticity also has a great influence on the rigid bridge, based on the simulation model to compare and analyze the deflection with different modulus of elasticity, the results are shown in Fig. 9.

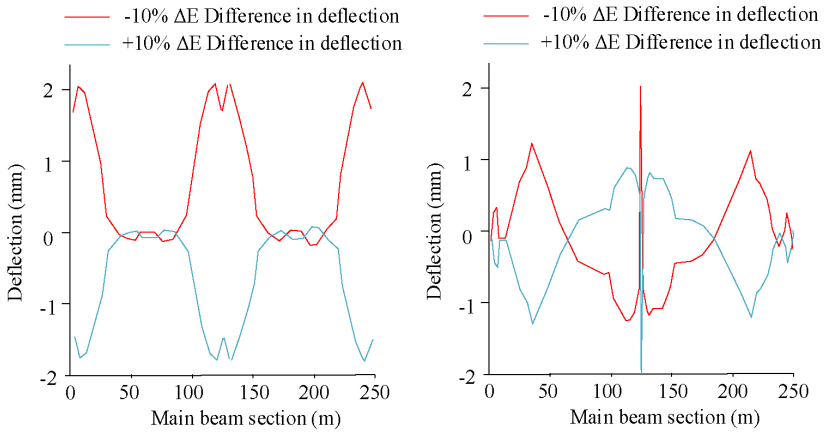

Fig. 9. Deflection analysis with different modulus of elasticity: (a) Difference in maximum cantilever state deflection for different modulus of elasticity, (b) Difference in deflection at bridge formation for different modulus of elasticity

Figure 9(a),(b) show the deflection difference between the maximum cantilever state and the bridge-forming state at different elastic modulus respectively. The overall comparison denotes that the deflection change of each node of the main girder is small when the concrete modulus of elasticity E is increased by 10% and mainly focuses on the side span and mid-span spans. The deflection difference in the maximum cantilever state is maximal at 2.1 mm, and that in the bridge-forming state is 1.5 mm. It can be analyzed and seen that the concrete modulus of elasticity has an effect on the deflection of the main girder. The analysis results of stresses under different elastic modulus are shown in Fig. 10.

Fig. 10(a),(b), show the stress difference between the upper and lower edges of the maximum cantilever state and the bridge-forming state at different elastic moduli, respectively. The overall comparison shows that in both states, the change of elastic modulus has a tiny effect on the stress and is symmetrical in the span with a maximum stress difference of 0.1 MPa. The analysis denotes that the change of elastic modulus of concrete has a very small effect on the

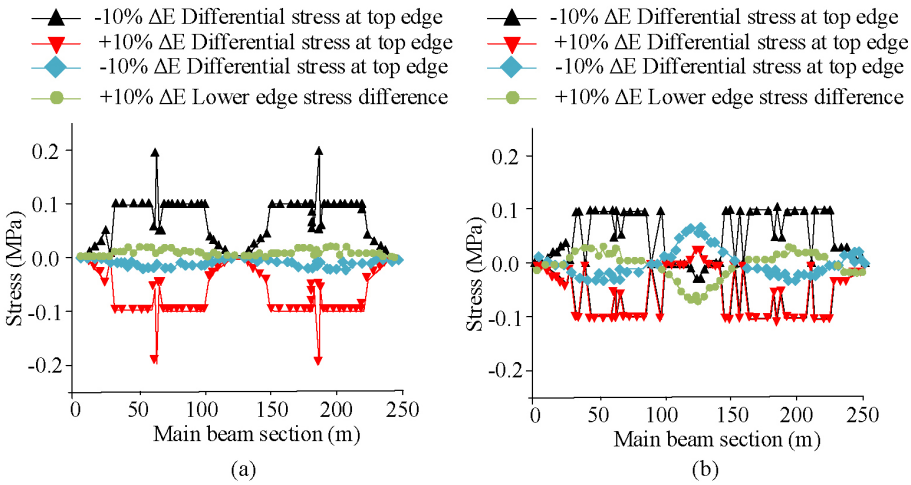

Fig. 10. Stress analysis with different modulus of elasticity: (a) Difference in stresses at the upper and lower edges of the maximum cantilever state for different moduli of elasticity, (b) Stress difference between the upper and lower edges of the bridge-forming state with different moduli of elasticity

stress. The deformation of concrete grows gradually under long-term continuous stress, which will have a large impact on the deformation and bearing capacity of concrete rigid bridge. However, there are many factors affecting the creep, and the study used the method of concrete component simulation experiment to determine the creep parameters of the rigid bridge in the research example. The comparison of the measured values of the creep test with the normative values and the fitting results are shown in Fig. 11.

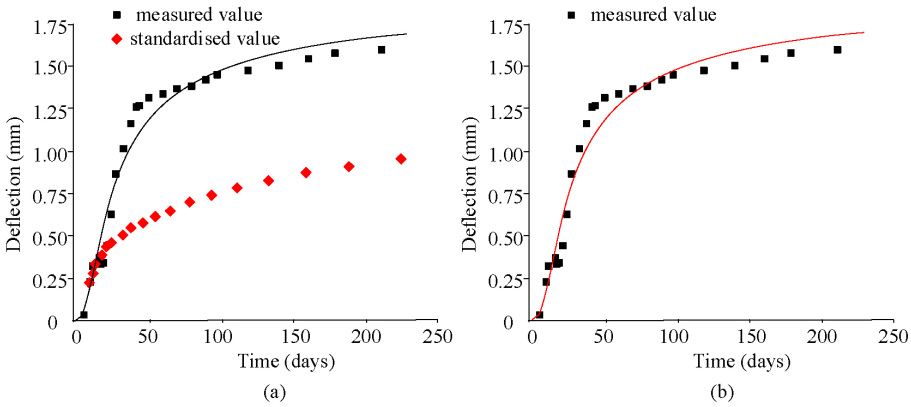

Fig. 11. Results of the creep test: (a) Normative values and test data, (b) Fitting curve of creep coefficient

As shown in Fig. 11, Fig. 11(a) represents the comparison between the measured value of the creep coefficient curve of C55 concrete and the specification value of the creep prediction model calibrated by JTG 3362-2018, and Fig. 11(b) shows the fitted curve of the creep

coefficient, which was fitted to the creep function of $y = 1.775 \times \left[\frac{x}{0.153 + x}\right]^{108.121}$, with a correlation coefficient of 0.96. The large difference between the test data of the mechanism sand concrete and the specification of JTG 3362-2018 stems from the fact that the JTG 3362-2018 specification's shrinkage creep model is based on the nonlinear regression correction of ordinary sand aggregate. There is a significant difference between the concrete formed by mechanism sand and ordinary sand, which is mainly caused by the higher content of stone powder in mechanism sand, the hydration of stone powder generates hydration crystals and increases the hydration products, so that the mechanism sand concrete slurry is more than the ordinary concrete. The loading test of 7-day age mechanism sand concrete shows that the creep deformation develops rapidly in the early stage, which affects the amount of creep. Finite element construction simulation of continuous rigid bridge according to JTG 3362-2018 specification may lead to the actual state error, which affects the precision of construction control. Linear control is a basic and intuitive control method for continuous rigid bridge construction, and the key lies in setting a reasonable pre-arch degree for the bridge. The size of pre-arch affects the accuracy of alignment control. The creep correction model, obtained through creep test, can accurately predict the deformation and stress of cantilever construction. With the increase of cantilever construction blocks, the model predicts more accurately, because the structural creep is the superimposed effect of the creep of the concrete poured before and after. The experimentally measured creep coefficients were input as parameter values for the FEA model, and the Midas FEA software was used to calculate the structural elevation, guide the construction and measure the elevation of each cantilever stage. If the error between the measured elevation and the theoretical value exceeds the limit, the source of error is analyzed and the model is adjusted to provide a more accurate elevation for the next section to ensure that the final structural alignment is consistent with the design. The bridge pre-arch correction based on the FEA model and the creep test results is expressed in Table 2. The experiment divided the bridge into 1–16 segments, and randomly selected cantilever segments for bridge pre arch correction. # represents the pre arch of the bridge before correction, and #'represents the pre arch of the bridge after correction.

Table 2. Bridge pre-camber correction

Serial number	Placement	Design elevation (m)	Original arch height (m)	Strain (mm)			Elevation of standing mold (m)
				projected value	standardized value	revised value	
1	Hualong section	556.54	0.13	12.44	5.99	6.55	556.62
2	Block 16#	556.55	0.14	3.62	–2.96	6.68	556.69
3	Block 15#	557.09	0.16	8.31	–0.21	8.41	556.78
4	Block 14#	557.13	0.17	8.01	0.71	7.41	556.83
5	Block 13#	557.16	0.17	7.19	0.95	6.34	556.94

Continued on next page

Table 2 – *Continued from previous page*

Serial number	Placement	Design elevation (m)	Original arch height (m)	Strain (mm)			Elevation of standing mold (m)
				projected value	standardized value	revised value	
6	Block 12#	557.21	0.17	6.49	1.06	5.53	557.09
7	Block 11#	557.32	0.17	6.18	1.26	5.03	557.12
8	Block 10#	557.35	0.17	5.60	1.25	4.45	557.17
9	10#' block	557.41	0.24	5.64	1.29	4.45	557.24
10	Block 11#'	557.46	0.24	6.23	1.31	5.03	557.29
11	12#' block	557.48	0.25	6.56	1.13	5.53	557.36
12	Block 13#'	557.52	0.26	7.36	1.11	6.35	557.42
13	14#' block	557.57	0.26	8.25	0.92	7.43	557.56

From Table 2, the modified model of creep obtained through the creep test can more accurately predict the deformation and stress of the cantilever construction of continuous rigid bridge. With the increase of cantilever construction blocks, the modified model can predict more accurately.

5. Conclusions

Cantilever construction is a commonly used construction method for large-span bridges, but its own instability makes alignment and stress control an important part of construction safety. To solve the linear and stress control problems of large-span PCCRF bridges in cantilever construction. The study is based on FEA to model the bridge case, and the research findings denoted that with the increase of structural deadweight, the deflection in the maximum cantilever state and bridge-forming state increases gradually. At a concrete capacity of 1.10 γ, the deflection change of the cantilever end of the main girder reaches its maximum value near the mid-span and side-span merging section, which is 8.6 mm and 9.7 mm, respectively. In the maximum cantilever condition, increasing the concrete capacity decreases the compressive stress at the upper and lower edge of the cross-section to 1.18 MPa and 1.24 MPa, respectively. In the completed condition, increasing the concrete capacity results in the decrease of positive stresses at the upper edge of the girder to 1.18 MPa, which is the highest value of the deflection at the mid-span and side-span merging section. When the modulus of elasticity of concrete E increases by 10%, the deflection change of each node of the main girder is small, which mainly focuses on the side span and the mid-span span, and the difference in deflection in the maximum cantilever state is 2.1 mm, and in the bridge-formed state it is 1.5 mm. The results of the creep test show that the creep function is $y = 1.775 \times \left[\frac{x}{0.153 + x}\right]^{108.121}$, and the correlation coefficient is 0.96, and the creep The modified model can more accurately

predict the deformation and stress of cantilever construction of continuous rigid bridge. As the increase of cantilever construction blocks, the modified model can predict more accurately. The FEA of the cantilever construction rigid bridge can predict the linear and stress changes for the purpose of controlling the linear and stress changes. The model proposed in the study provides new tools for stress analysis and cantilever structure changes in the bridge construction industry by predicting linear and stress changes through finite element analysis, promoting the development of the bridge description industry.

References

[1] D. Wu, W. Xiong, and J. Guo, "Establishment and repetition survey of primary GNSS control network of Hong Kong-Zhuhai-Macao bridge", *Journal of Surveying Engineering*, vol. 148, no. 1, pp. 1006–1017, 2022, doi: 10.1061/(ASCE)SU.1943-5428.0000386.

[2] Q. Su, Y. Zhu, Y. Chen, et al., "Hong Kong Zhuhai Macao Bridge-Tunnel project immersed tunnel and artificial islands - From an owners' perspective", *Tunneling and Underground Space Technology*, vol. 121, pp. 308–326, 2022, doi: 10.1016/j.tust.2021.104308.

[3] M.K. Hoke, "A biocultural examination of home food production and child growth in highland Peru", *American Journal of Human Biology*, vol. 32, no. 4, pp. 438–442, 2020, doi: 10.1002/ajhb.23438.

[4] S. Reymert, A. Rönnquist, and O. Øiseth, "Systematic metadata analysis of wind-exposed long-span bridges for road vehicle safety assessments", *Journal of Bridge Engineering*, vol. 27, no. 2, pp. 104–111, 2022, doi: 10.1061/(ASCE)BE.1943-5592.0001822.

[5] T. Siwowski, M. Rajchel, and M. Kulpa, "Design and field evaluation of a hybrid FRP composite - Lightweight concrete road bridge", *Composite Structures*, vol. 230, pp. 504–523, 2019, doi: 10.1016/j.compstruct.2019.111504.

[6] C. Ma, "Physical properties and durability of green fiber-reinforced concrete for road bridges", *Annales de Chimie-Science des Materiaux*, vol. 45, no. 2, pp. 181–189, 2021, doi: 10.18280/ACSM.450211.

[7] B. Dai, D. Wu, and Q. Li, "Investigation of multiple-presence factor for traffic loads on road-rail bridges based on a novel extreme value analysis approach", *Structural Safety*, vol. 96, pp. 199–214, 2022, doi: 10.1016/j.strusafe.2022.102199.

[8] E. Cosenza and D. Losanno, "Assessment of existing reinforced-concrete bridges under road-traffic loads according to the new Italian guidelines", *Structural Concrete*, vol. 22, no. 5, pp. 2868–2881, 2021, doi: 10.1002/suco.202100147.

[9] Y. Zhu, J. Liu, X. Li, J. Li, L. Zhang, and B. Li, "Improving the temperature stability of superelastic stress of Cu-Al-Mn shape memory alloy in a wide temperature range by torsion pre-deformation", *Materials Letters*, vol. 341, no. 15, pp. 214–218, 2023, doi: 10.1016/j.matlet.2023.134214.

[10] M. Sarmah, S.K. Deb, and A. Dutta, "Hybrid simulation for evaluation of seismic performance of highway bridge with pier retrofitted using Fe-SMA strips", *Journal of Bridge Engineering*, vol. 28, no. 8, pp. 50–67, 2023, doi: 10.1061/jbenf2.beeng-6047.

[11] Z. Kang, Z. Zhang, S.Y. Song, Q. Cheng, S. Tao, and Y. Ni, "Effect of pitting corrosion on the mechanical properties and fracture model of steel wires for bridge cable", *Anti-Corrosion Methods and Materials*, vol. 70, no. 4, pp. 173–181, 2023, doi: 10.1108/acmm-02-2023-2763.

[12] G. He, Y. Li, Z. Zou, and L. Duan, "Effect of concrete creep on pre-camber of continuous rigid-frame bridge", *Journal of Central South University of Technology*, vol. 15, no. s1, pp. 337–341, 2008, doi: 10.1007/s11771-008-0376-1.

[13] L. Tong, D. Wang, Z.G. Sun, L. Chen, and F. Shi, "Seismic uplift effect at end spans of long-span rigid-frame bridges subjected to near-fault and far-fault ground motions", *Journal of Bridge Engineering*, vol. 28, no. 7, pp. 230–249, 2023, doi: 10.1061/jbenf2.beeng-6023.

[14] S. Yao, B. Peng, L. Wang, and H. Chen, "Estimation formula of fnished bridge precamber in continuous rigidframe bridges", *Scientifc Reports*, vol. 12, art. no. 16034, 2022, doi: 10.1038/s41598-022-20449-4.

[15] S. Cui, C. Guo, G. Zeng, L. Xu, J. Ju, and H.Y. Jia, "Influence of hydrodynamic pressure on fragility of high-pier continuous rigid frame bridge subjected to ground motion", *Ocean Engineering*, vol. 264, pp. 682–692, 2022, doi: 10.1016/j.oceaneng.2022.112516.

[16] L. Sun, Y. Liu, H. Wang, F. Shi, J. Liu, L. Jiang, "Tensile stiffness of perfobond rib connectors in steel-concrete composite pylon of bridges", *Engineering Structures*, vol. 284, pp. 3–14, 2023, doi: 10.1016/j.engstruct.2023.115931.

[17] Y. Liu, C. Zheng, H. Ba, G. Xu, C. Li, and Q. Xie, "Analysis on the influence factors of construction linear control of continuous rigid structure bridge", *E3S Web of Conferences*, vol. 237, art. no. 03020, 2021, doi: 10.1051/e3sconf/202123703020.

[18] S. Sun, L. Xing, P. Gui, B. Li, H. Li, L. Zhao, and K. Mei, "Experimental study on the bond performance of steel-basalt fiber composite bars in concrete", *Journal of Composites for Construction*, vol. 27, no. 2, pp. 2–15, 2023, doi: 10.1061/jccof2.cceng-3612.

[19] M. Cai, W. Li, Z. Wan, J. Sheng, J. Tan, and C. Ma, "Cracking control technique for continuous steel-concrete composite girders under negative bending moment", *Archives of Civil Engineering*, vol. 69, no. 3, pp. 239–251, 2023, doi: 10.24425/ace.2023.146078.

Received: 2023-11-24, Revised: 2024-04-16